Loughborough University

This item was submitted to Loughborough's Research Repository by the author.
Items in Figshare are protected by copyright, with all rights reserved, unless otherwise indicated.

Compact latent heat storage decarbonization potential for domestic hot water and space heating applications in the UK

PLEASE CITE THE PUBLISHED VERSION

https://doi.org/10.1016/j.applthermaleng.2018.01.120

PUBLISHER

Elsevier

VERSION

AM (Accepted Manuscript)

PUBLISHER STATEMENT

This work is made available according to the conditions of the Creative Commons Attribution 4.0 International (CC BY 4.0) licence. Full details of this licence are available at: http://creativecommons.org/licenses/ by/4.0/

LICENCE

CC BY 4.0

REPOSITORY RECORD

da Cunha, Jose M.P. Pinto Pereira, and Philip Eames. 2018. “Compact Latent Heat Storage Decarbonization Potential for Domestic Hot Water and Space Heating Applications in the UK”. Loughborough University. https://hdl.handle.net/2134/28427.

Applied Thermal Engineering 134 (2018) 396–406

Contents lists available at ScienceDirect

Applied Thermal Engineering

journal homepage: www.elsevier.com/locate/apthermeng

Compact latent heat storage decarbonisation potential for domestic hot water and space heating applications in the UK

Jose Pereira da Cunha*, Philip Eames

Loughborough University, Wolfson School of Mechanical, Electrical and Manufacturing Engineering, Loughborough, Leicestershire LE 11 3TU, United Kingdom

HIGHLIGHTS

- PCM store with air source heat pump comparison to gas boiler for DHW and SH.
- Both systems integrated into semi-detached dwelling in typical UK midlands climate.
- PCM store system reduced yearly CO2 emissions by 56% and consumed 76% less energy.
- PCM store system LCOE was 117.84£/MWh, compared to 69.66£/MWh for the gas boiler.

ARTICLE INFO

Keywords:
Phase change materials
Latent heat thermal storage
Domestic hot water
Domestic space heating
Air source heat pumps, finite volume enthalpy models

ABSTRACT

A performance comparison is presented for a domestic space and hot water heating system with a conventional gas boiler and an air source heat pump (ASHP) with latent heat storage, both with solar thermal collectors for a typical UK climate, to demonstrate the potential of phase change material based energy storage in active heating applications. The latent heat thermal storage system consisted of 10 modules with RT54HC comprising a total storage capacity of 14.75 kWh that provided 53% extra thermal storage capacity over the temperature range of 40–65 °C compared to a water only store. The simulations predicted a potential yearly CO_2 reduction of 56%, and a yearly energy reduction of 76% when operating the heat pumps using the economy 10 electricity tariff i.e. a low tariff between 00.00 and 05.00 and 13.00–16.00 with current grid emission values compared to the conventional gas boiler system; successfully offsetting the electrical load to meet the required heat demand. Due to the high capital costs of the heat pump system with latent heat storage, its levelized cost of energy was 117.84£/MWh, compared to 69.66£/MWh for the gas boiler, on a 20-year life cycle.

1. Introduction

Approximately 18% of the UK's final energy consumption in 2016 was used for domestic water heating, mainly through the use of natural gas boilers [1], totalling 26773 mtoe. In order to decarbonize the sector, the use of renewable heat sources such as solar thermal could be implemented, backed up by either heat pumps or gas boilers. Heat pump operation should, where possible, be restricted to off peak times to prevent an increase in the peak electrical grid demand [2].

Fig. 1 presents the UK national grid emissions on each season of 2016 [3]. The CO_2 emissions associated with each generation profile were calculated based on the emission coefficients obtained by Hawkes [4].

To effectively decarbonize this sector, heat pump CO_2 emissions should be less than the currently used conventional gas burning domestic heating systems (around 204 g CO_2/kWh_{th} [4,5]), and operated during off peak electrical load times to minimise both carbon intensity and peak electrical load. This can be achieved if heat pumps are operated using either economy 10 or economy 7 electricity tariffs [5], with hot water buffer tanks used to store heat, offsetting the electrical load while meeting the heat demand required.

The higher CO_2 grid emissions during the winter months are mainly due to the higher consumption of coal and natural gas, consequence of a larger electrical demand by the UK grid. It can be seen in Fig. 1 that the lowest CO_2 daily emission period is from 23.00 to 05.00 and a depression in the marginal emissions curve occurs from 12.00 to 16.00 in all seasons.

Hot water tanks have nearly constant heat capacity over the working temperature range of 40–65 °C [6], typical temperature band for domestic hot water and space heating, hence requiring a considerable volume to buffer some of that daily heat demand.

* Corresponding author.
E-mail addresses: j.pereira-da-cunha@lboro.ac.uk (J.P. da Cunha), p.c.eames@lboro.ac.uk (P. Eames).

https://doi.org/10.1016/j.applthermaleng.2018.01.120
Received 25 May 2017; Received in revised form 9 January 2018; Accepted 30 January 2018
Available online 01 February 2018
1359-4311/ Crown Copyright © 2018 Published by Elsevier Ltd. This is an open access article under the CC BY license (http://creativecommons.org/licenses/BY/4.0/).

Nomenclature

di [m]	tube inner diameter
do [m]	tube outer diameter
H_{stored} [kWh/m^3]	volumetric heat stored
L [m]	tube length
Nu	Nusselt Number
Pr	Prandtl Number
Ra	Rayleigh Number
Re	Reynolds Number
ρ	[kg/m^3] – densityV
μ [Pa s]	dynamic viscosity
λ [W/m K]	thermal conductivity
ζ [m^2/s]	kinematic viscosity
σ	Stephan-Boltzmann constant
ξ [mm/mm]	relative surface roughness
g [m^2/s]	earth's gravitational acceleration
[C]	capacitance matrix
[Γ]	transport matrix
{T}	nodal temperatures vector
{F_{out}}	external nodal energy transfer vector
Ti,j [°C]	Nodal temperature

2. PCM screening and characterization

Phase change materials (PCMs) with a phase transition temperature between 50 and 60 °C can effectively be used to increase thermal storage capacity in that narrow temperature, hence reducing the required storage volume achievable with hot water buffer tanks. Commercial organic PCMs melting in this temperature range are Paraffin waxes (RT52, RT54HC [7]) and fatty acids, such as the eutectic mixture of stearic and palmitic acids (36/64%wt) studied by Baran and Sari [8]. Salt hydrates are other candidate PCMs, however their high subcooling usually prevents them from working successfully in a narrow temperature range.

The paraffin wax RT54HC, the eutectic mixture of stearic acid-palmitic acid [8] (36/64%wt) and the eutectic mixture of magnesium nitrate hexahydrate and magnesium chloride hexahydrate (41/59%wt) were prepared experimentally and their specific heat capacity determined using differential scanning calorimetry (DSC). Table 1 presents the thermophysical properties of the 3 PCMs characterized. It can be seen that the salt hydrate eutectic mixture is nearly 3 times more energy dense than the same volume of water, within the 40–65 °C temperature range.

The heat capacity thermograms presented in Fig. 2 were determined experimentally using the TA instruments Discovery differential scanning calorimeter [16] at 2 different temperature ramp rates, 1 and 10 °C/min [17], using the faster ramp rate as reference for the solid and liquid heat capacities and using the resolution of the slower ramp rate for the thermogram.

3. Developed numerical model

A 2D finite volume model was developed to simulate a compact latent heat energy storage system, similar to the tubular array studied by Nakaso et al. [18] in Matlab. The numerical model assumed isotropic heat propagation within the PCM, having temperature-dependent thermal conductivity and volumetric heat capacity [J/m^3 K] with no volume changes occurring during phase change.

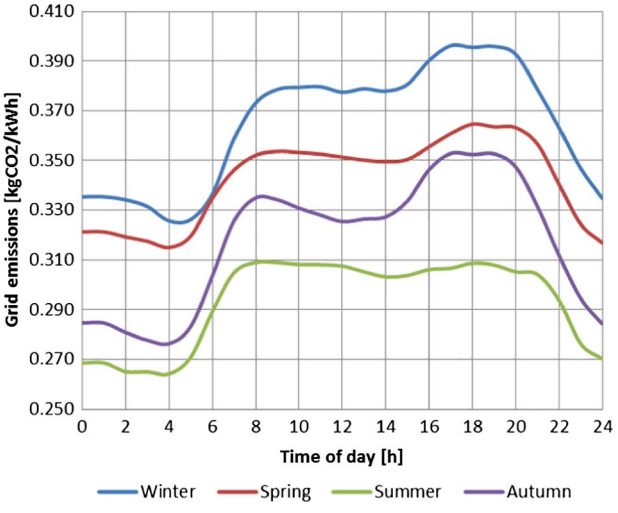


Fig. 1. Hourly variation of CO_2 emissions associated with the electricity supplied by the UK national grid [3] on each season of 2016.

The compact tube-in-tube simulated a long copper string inserted into a rectangular PCM slab, as illustrated in Fig. 3A. In order to meet the required storage capacity, the model added numerous strings in parallel connected through a larger diameter copper manifold pipe, distributing the water flow evenly throughout the multiple strings, seen schematically in Fig. 3B. The model employed backward spatial discretization for the water flow, and unidirectional radial and axial heat propagation among the copper tube and PCM, as it is presented schematically in Fig. 3C and D.

The container's heat loss to ambient was accounted to the last PCM node outer surface, determined using the insulation properties specified in the container (insulation thickness, type and ambient temperature) and divided by the number of axial nodes and strings. The simulated charge and discharge of the container represented a fluid flowing in the inner tube, exchanging heat by convection with the tube inner surface.

The Heat Transfer Fluid (HTF) Reynolds number was calculated using Eq. (1), for pipe flow. For laminar flows, the average Nusselt Number was obtained considering a constant wall temperature, according to the correlation from [19], expressed in Eq. (4). For fully turbulent flows, with a Reynolds number above 10,000, Nusselt numbers were obtained with the correlation put forward by Gnielinski [19], expressed in Eq. (5). For transitional flows, a linear interpolation (Eq. (3)) between the laminar and turbulent regimes was adopted, Eq. (2).

$$Re = \frac{4 \times \rho_{htf} \times Q}{\pi \times \mu_{htf} \times d^2} \tag{1}$$

$$Nu_{trans} = f \times Nu_{lam,2300} + (1-f) \times Nu_{turb,10000} \tag{2}$$

$$f = \frac{Re-2300}{7700} \tag{3}$$

$$Nu_{lam} = \left\{ 3.66 + 0.7^3 + \left[1.615\sqrt[3]{Re \times Pr \times \frac{d}{L}} - 0.7 \right]^3 + + \left[\left(\frac{2}{1+22Pr} \right)^{\frac{1}{6}} \sqrt{Re \times \mathrm{Pr} \times \frac{d}{L}} \right]^3 \right\}^{\frac{1}{3}} \tag{4}$$

$$Nu_{turb} = \frac{\frac{\xi}{8} \times Re \times Pr}{1 + 12.7 \times \sqrt{\frac{\xi}{8}} \times \left(Pr^{\frac{2}{3}} - 1 \right)} \left[1 + \left(\frac{d}{l} \right)^{\frac{2}{3}} \right] \tag{5}$$

The developed numerical model calculated new mass and transport matrices at each time step to enable the transient accounting for changes in the PCM's heat capacity (phase change) and thermal conductivity.

Some of water's thermophysical properties (namely viscosity and the Prandtl number) were also temperature dependent, due to the

Table 1
Properties of PCMs selected for potential use in space heating applications.

PCM	ΔT °C	H_{stored} kWh/m^3	H/H_{H2O} kWh/kWh	λ mW/m K		Price £/kWh
41%$MgCl_2.(H_2O)_6$ + 59%$Mg(NO_3)_2.(H_2O)_6$ (SH-SH)	40–65	78	2.72	600	606	1.19 [9,10]
36%stearic acid + 64%palmitic acid (SA-SPA) [8]		61	2.11	288	168	5.72 [11,12]
RT 54HC [7]		52	1.80	215 [13]	165 [14]	7.63 [15]

changes in the convective heat transfer coefficient. The spatial discretization, seen in Fig. 3C and D, employed 9 radial nodes and 40 axial nodes giving a modelled cylinder height to thickness ratio between 125 and 170.

Eq. (6) presents the three set of equations used to compute the solution during each time step ($[\Gamma_1]$ the transport matrix, [C] the mass matrix, f_t is a variable ranging from 0 to 1 that can be used to tune the algorithm from an explicit to an implicit approach), all models were solved implicitly. The term $\{F_{out}\}$ accounts for the inlet mass flow. Matlab uses a Gauss-Seidel iterative solver to obtain the new temperature distribution in each time step.

$$\begin{cases} [\Gamma_2] = f_t . [\Gamma_1] + [C] \\ \{m_1\} = (1-f_t) . [\Gamma_1] \times \{T_{old}\} + [C] \times \{T_{old}\} + \{F_{out}\} \\ \{T_{new}\} = [\Gamma_2]^{-1} \times \{m_1\} \end{cases} \quad (6)$$

3.1. Model verification

A compact latent heat storage module was developed in situ to investigate the thermal performance of PCMs in a rectangular slab. The rectangular slab was made from 3 mm aluminium sheet bolted to four 1.5″ aluminium C profiles. A ½″ copper pipe string was inserted within the slab to exchange heat between the water flow and the PCM. The copper string comprised 39 U-bends soldered to 511 mm tube sections. Copper metal fins were soldered to the tube outer surface to improve heat transfer among the PCM. A simplified view of the rig is displayed in Fig. 4A.

The rectangular storage contained 18.3L of RT44HC [7], able to store 1.39kWh$_{th}$ when heated/cycled from 20 to 70 °C. The storage general dimensions and main characteristics are presented in Table 2. Water is used as the heat transfer fluid, while the PCM (RT44HC [7]) occupies the spaces around the pipe within the rectangular tank. The PCM slab is inserted within a 12 mm thick MDF enclosure (thermal conductivity 0.151 W/m K) with 20 mm air gaps between the container sides, as seen in Fig. 4B. Using 5 copper fins spaced 32 mm and soldered transversally to the copper pipe increased the total heat transfer area within the PCM by 52%.

A Huber Unistat tango was used to indirectly exchange heat with the water rig, using a programmable proportional-integral-derivative (PID) controller to maintain the set point temperature constant during charging and discharging the store. Thermocouples are fixed at the HTF inlet and outlet of the thermal store. The PCM temperature is monitored using thermocouples positioned at the 2 locations presented in Fig. 4A, and the flow rate is monitored by a turbine flow meter from Icenta, its signal converted to current and read in a compact DAQ card from

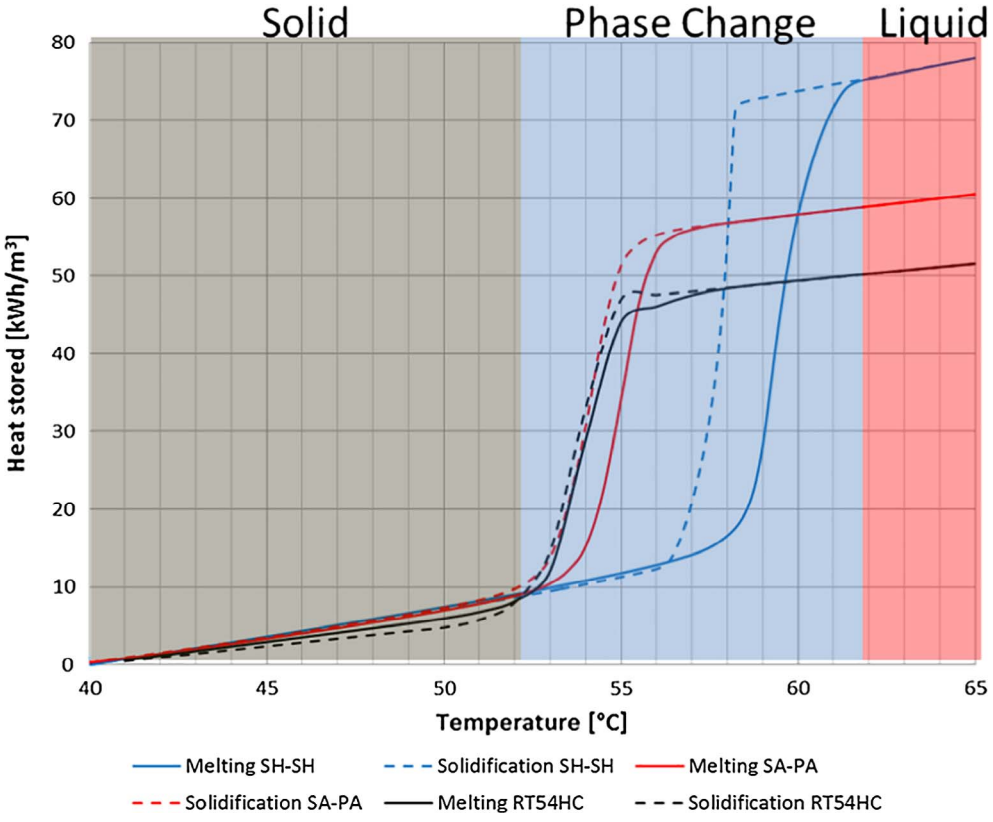


Fig. 2. Heat capacity thermograms for the three selected PCMs determined experimentally at a ramp rate of 1 °C/min.

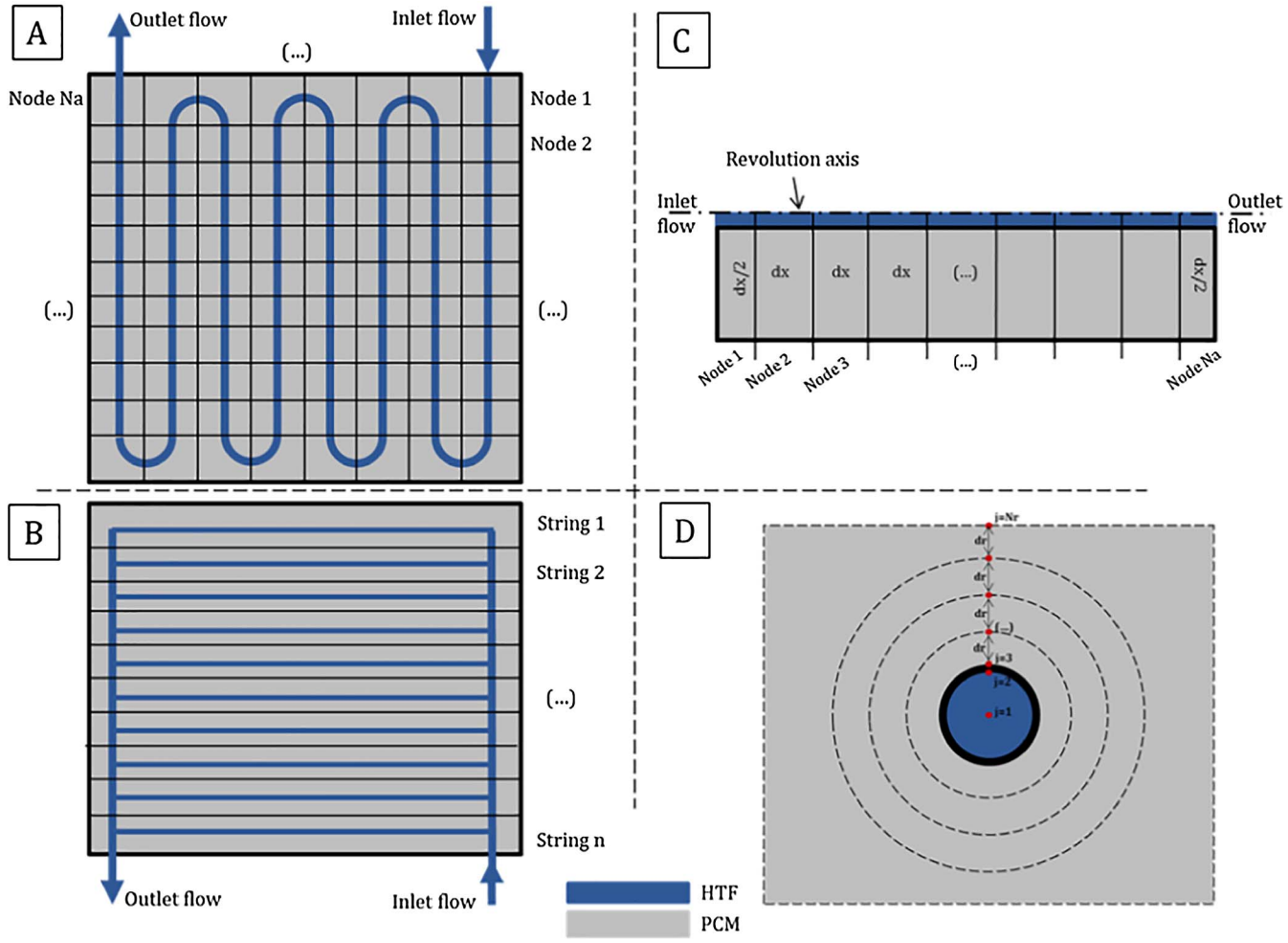


Fig. 3. Cross section view of a single string (A), top view of the parallel of strings per module (B) representation of the axial discretization in each tubular string (C) and transversal discretization in each node (D).

National Instruments.

The experiment is carried out in two modes: charging and discharging. For the charging mode, the initial state of the PCM is solid at room temperature of 20.3 °C. The HTF is heated in the shell and tubes heat exchanger and pumped through the copper pipe. The charging is completed when all the PCM in the tank has melted fully and its temperature has stabilized around 70 °C, with temperature readings taken every minute. For the discharging mode, the HTF temperature is dropped to 20 °C and temperature readings continue until the PCM temperature has stabilized around 20 °C. Fig. 5 presents the comparison between experimental results and modelled numerical results obtained for the temperature profiles. The thermal store had fully melted at 180 min, as can be seen in Fig. 5.

Fig. 6 presents the comparison between the experimental results and modelled simulation results obtained for the heat rate profiles. The heat rate had a charging plateau around 800 W and a slightly lower discharge plateau around 700 W. Due not accounting buoyancy driven convection currents in the molten PCM, the temperature evolution in the charging cycle was slower than expected, as seen in Fig. 6A. That led to a lower charging rate and consequently less energy charged.

To address this, a theoretical conductivity increase resulting from buoyancy forces was calculated based on the Rayleigh number for the temperature difference between the PCM's melting point and the node temperature, expressed in Eq. (7). The Nusselt number can then be calculated using the correlations for free convection on a vertical annulus [19], Eq. (8), and calculated for each PCM node to give the required addition to the conductivity. The annulus height considered was the fin's spacing and the annulus thickness half the spacing between tubes.

$$Ra_{i,j} = \frac{g \times \beta \times s_{i,j}^3 \times (T_{i,j} - T_m)}{\zeta^2} \times Pr_{i,j} \tag{7}$$

$$Nu_{Ra} = \frac{0.49 \times Ra\left(\frac{H_{fin}}{0.5 \times L_{fin} - r_{tube}}\right)^2}{862 \times \left(\frac{H_{fin}}{0.5 \times L_{fin}}\right)^4 \left(\frac{r_{tube}}{H_{fin}}\right) + \left[Ra\left(\frac{H_{fin}}{0.5 \times L_{fin} - r_{tube}}\right)^3\right]^{0.95} \left(\frac{r_{tube}}{H_{fin}}\right)^{0.8}} \tag{8}$$

It can be seen from Fig. 6A and B that the inclusion of additional conductivity to account for buoyancy driven convective currents in the PCM led to a more accurate prediction of the PCM's melting process, with the predicted water flow outlet temperature in better accordance with the experimental measurements. From the discharge profiles, the PCM's conductivity increase has negligible effect in the water flow inlet/outlet temperature difference, mainly because the driving buoyancy force is nearly suppressed, with both predictions following the experimental results accordingly.

3.2. System design and integration

Following the parametric analysis, the latent heat store was integrated into a simulation of a domestic heating system, illustrated schematically in Fig. 7. An air source heat pump was used as the heat source, working during off peak hours based on economy 10 electricity

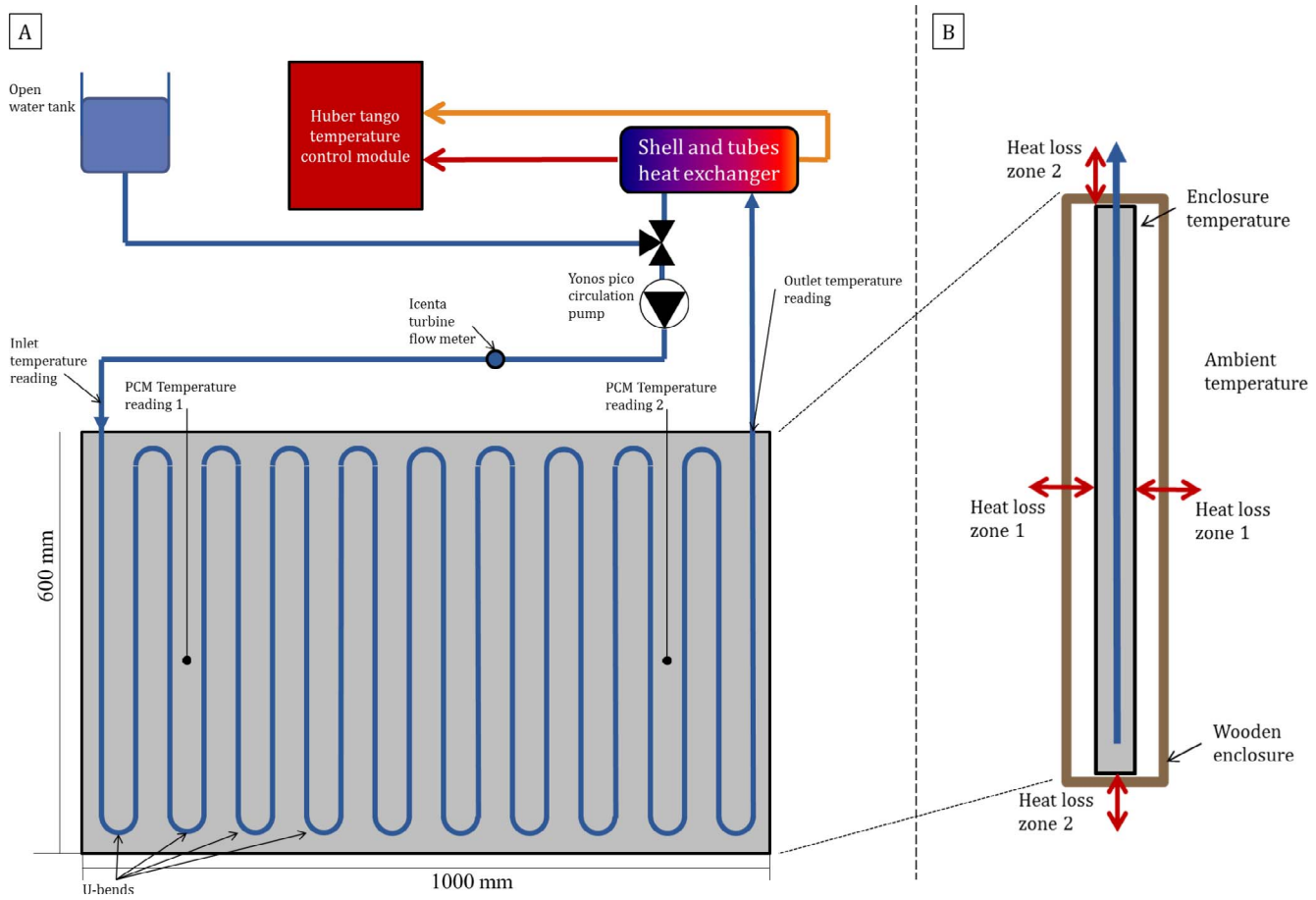


Fig. 4. Experimental rig used with RT44HC [7] and simplified view of the thermocouples and flow meter distribution.

Table 2
Store dimensions, heat transfer fluid flow and storage material properties for the experimental work performed.

PCM slab width [mm]	600	Volume [L]	21.3
PCM slab length [mm]	950	PCM volume [L]	19.0
PCM slab thickness [mm]	37	Number of fins	18
Coil length [m]	12.14	PCM fraction [%]	88.9
Tube OD (ID) [mm]	15.86 (12.45)	Specific HT area [m^2/m^3_{PCM}]	48.23
HTF (average values):		PCM (RT44HC)	
Flow rate [g/s]	148.10	H_{sl} (37–46 °C) [kWh/m^3]	49.57
Re	24 603	Cp_s (20–37 °C) [MJ/m^3 K]	1688.4 + 1.6211 * T
Pr	4.28	Cp_l (46–70 °C) [MJ/m^3 K]	1323.5 + 9.7665 * T
Nu	153	λ_s (20–37 °C) [W/m K]	0.450–0.00096 * T
(h_{cv}) [W/m^2 K]	7249	λ_l (46–70 °C) [W/m K]	0.188–0.00036 * T

tariffs (00.00–05.00/13.00–16.00) [5], using the characteristics of a Daikin Altherma V high temperature air source heat pump [20] in the simulation. Two solar flat plate thermal collectors were coupled to the system in the simulation to provide a near-zero carbon heat source and to compare the solar fraction gains in utilizing a thermal store, its characteristics are summarized in Table 3.

The latent heat system was sized to meet the highest heat demand for a semi-detached dwelling over a period of 8 h during the predicted simulation for winter conditions, with paraffin wax RT54HC [7]. The reason for using Paraffin wax as the PCM was due to the developed numerical model being verified for a similar wax. The building fabric thermal performance was considered improved by insulation retrofit compared to a conventional 1930 semi-detached dwelling. The reason for selecting this type of dwelling is due to its importance, since it represented a quarter of the British housing stock in 2015, around 6 million dwellings, based on the English housing survey report made by the Department for Communities and Local Government [22].

The 80L hot water tank would be charged in off peak hours with the circulating pump P1 (20 L/min maximum). If the solar thermal collector temperature was 1 °C above the hot water tank, solar circulator pump P3 (2 L/min per collector) would directly charge the hot water tank, as presented in Fig. 7. The reason for using a small hot water tank would be to compensate the temperature drop of the latent heat store in periods of high heat demand consequence of having a low water volume within the latent heat store.

The household space heat distribution system would be met by circulating pump P2 (12 L/min) transferring heat directly from the hot water tank to the household, shown schematically in Fig. 7. When indoor temperature dropped 0.5 °C below the set point, P2 would be activated until it achieved an indoor temperature 0.5 °C above the set point. Whenever a hot water appliance was activated, valve V1 would open and thermostatic valve Vt would regulate the hot water flow coming from the hot water tank to maintain a constant 38 °C temperature output.

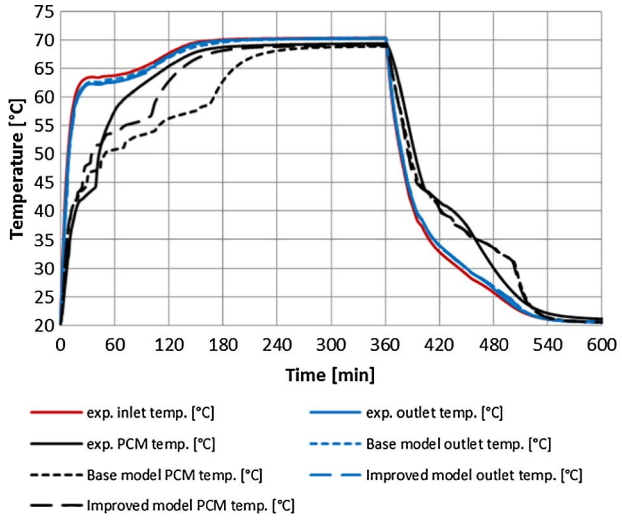


Fig. 5. Comparison between experimental and simulation results for the temperature profiles.

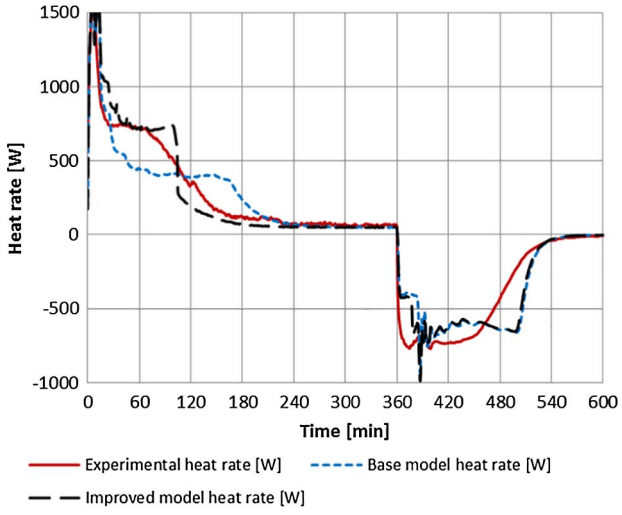


Fig. 6. Comparison between experimental and simulation results for the heat rate profiles.

The compact latent heat store, comprising 79% of the total heat storage capacity from 40 to 65 °C would be connected with the radiator end temperature and cold-water inlet, in order to maintain the highest thermal stratification possible. Table 3 presents also the dwelling and collector thermal properties and daily energy spent for space heating and domestic hot water per season. The higher energy use occurs during the winter months, being the thermal store sized to meet those heat demands, over sizing it during the remaining months.

To estimate daily carbon emissions released in the heating system, the marginal CO_2 grid emissions used were based in the study of Hawkes [4], presented in Fig. 1. To determine the heat pump's coefficient of performance (COP), technical data sheets for the Daikin Altherma V were used [23] with a 65 °C outlet temperature assumed, including the effect of defrost cycles.

Fig. 8 presents the balance equations for the 5 extra nodes added to the latent heat store to simulate the hot water tank volume (A and B), the solar thermal collector volume (C) the house heat emitter volume (D) and the household indoor volume (E). The two balance nodes for the hot water tank were due to the reversibility of the water flow coming from the latent heat store. Stratification within the hot water tank is not taken into account due to the reduced size of the tank, as seen in Fig. 8A and B.

The convective heat transfer coefficient of the heat emitters (Eq. (11)) was determined during each time step by calculating the Rayleigh number (Eq. (9)) and Nusselt coefficient for a vertical surface (Eq. (10)) using the instantaneous emitter-ambient temperature difference, and considering a typical emitter height of 600 mm [6]. The radiative heat transfer coefficient, assuming the heat emitter area much smaller than the household's walls and a surface emissivity of 0.95, can be calculated according to Eq. (12) using also the instantaneous emitter-ambient temperature, from [19]. The emitter global heat transfer coefficient, seen in Fig. 8D and E, would be the sum the 2 coefficients, seen in Eq. (13). The convective heat transfer coefficient is multiplied by 2 since convection occurs on the 2 sides of the heat emitter.

$$Ra_{(t)} = \frac{g \times \beta \times h^3 \times (T_{amb}(t) - T_{em}(t))}{\zeta^2} \times Pr_{air} \tag{9}$$

$$Nu_{Ra} = \left(0.825 + 0.387\left(Ra\left(1 + \left(\frac{0.492}{Pr}\right)^{\frac{9}{16}}\right)^{-\frac{16}{9}}\right)^{\frac{1}{6}}\right)^2 \tag{10}$$

$$h_{cv} = \frac{Nu \times \lambda_{air}}{L_{emitter}} \tag{11}$$

$$h_{rad} = \sigma\varepsilon_{emitter}(T_{amb}^2 + T_{emitter}^2)(T_{amb} + T_{emitter}) \tag{12}$$

$$UA_{emitter} = A_{emitter}(2 \times h_{cv} + h_{rad}) \tag{13}$$

The designed latent heat storage module developed was able to store 255L of PCM material with 10 strings connected in parallel. Using off-the-shelf copper pipe accessories, each string had a 11.56 m ½″ nominal size copper tube string, with 37 U-bends, as presented in Fig. 9A. All 10 strings would then be connected to a larger copper manifold, ensuring an even flow distribution, as seen in Fig. 9B.

With the RT54HC [7] (properties summarized in Table 1), occupying around 67% of the total storage system volume, its total thermal energy storage capacity increased by 53% compared to the same store volume using only water, between 40 and 65 °C, due to the latent heat capacity of the PCM between 52 and 56 °C, as shown in Fig. 2. Table 4 presents the geometrical properties of the modelled latent heat storage. Using 18 fins per string increased the specific heat transfer area by 387%.

Having 10 strings within the store allowed the heat transfer fluid flow to be divided by the same factor in the ¾″ manifold pipe, as it can be seen in Fig. 9B. That would result in reducing the Reynolds number when charging from the heat pump from 30,000 (fully turbulent) to 5800 (turbulent), reducing subsequently pipe head losses from 54 kPa to 63 Pa.

4. Results

Fig. 10 presents the predictions of heat supplied for the dwelling in a winter and summer day, using McKenna's high-resolution stochastic model [21].

In these simulations, there is a significant variance in the dwellings indoor temperatures around the set point temperatures, consequence of having wider boiler set point temperatures (varying from 15.1 to 24.4 °C for the winter climate predictions). During spring, summer and autumn months, the solar thermal collector temperature went above 100 °C due to having the DWH tank cut off temperature at 70 °C and insufficient thermal capacity to store available daily solar energy below 70 °C, leading to a significant loss of solar thermal energy.

The predicted temperatures and heat supply rates from simulations using the developed model are presented in Fig. 11.

This model predicts more rapid indoor temperature variations mainly resulting due to the narrow temperature control band (± 0.5 °C), which leads to more variations in the heat emitter temperatures.

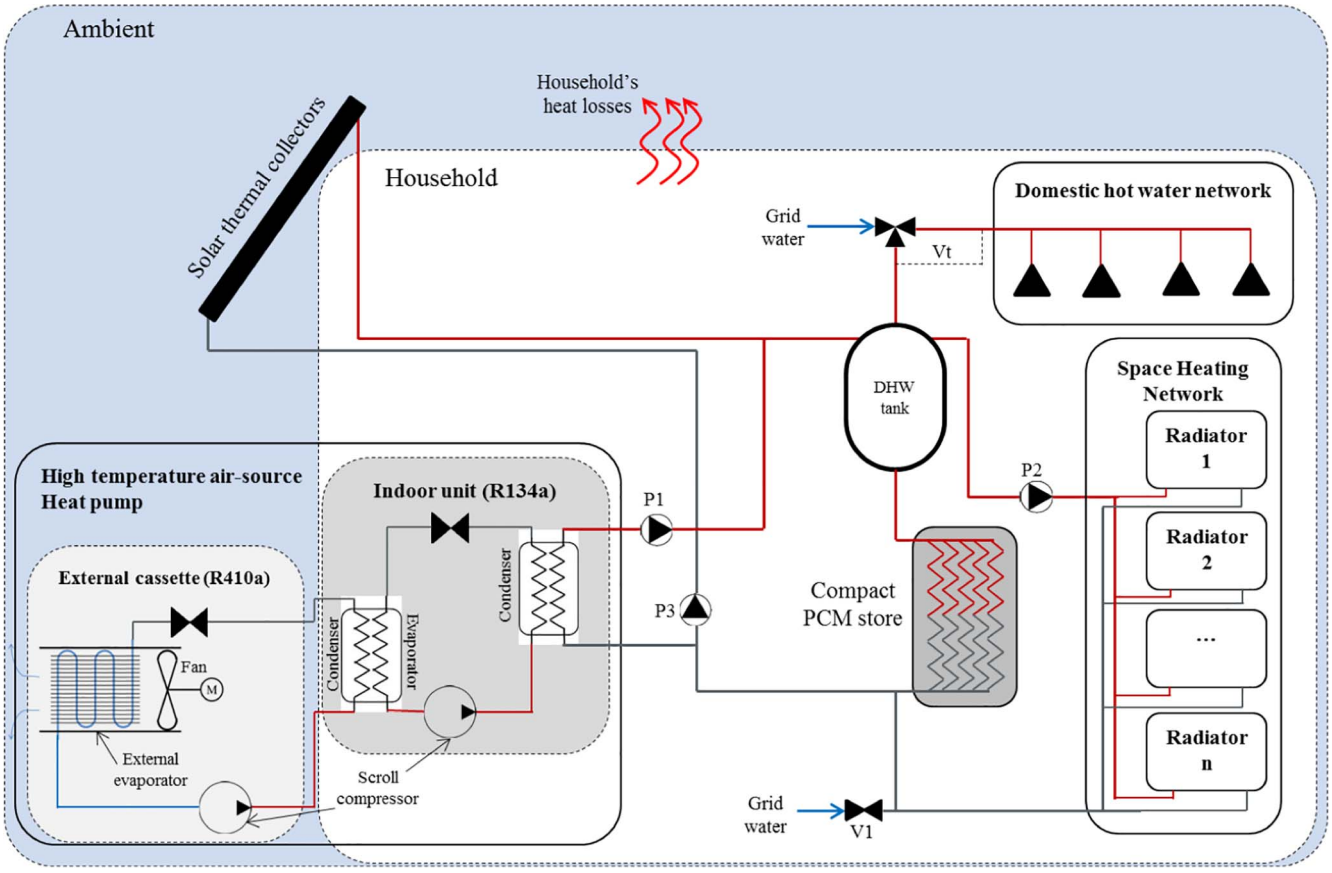


Fig. 7. Schematic representation of the latent heat store integrated into a conventional domestic heating system.

Table 3
Dwelling properties employed to predict system performance from Mckenna et al. [21].

Season	Winter	Spring	Summer	Autumn	Units
SH Demand	27.22	7.65	0.64	2.73	kWh
DHW demand	6.40	6.90	6.16	7.01	
Solar daily use	1.76	4.30	8.66	5.52	
Required 8 h storage capacity	12.29	7.12	4.45	4.63	
Daily hot water used (60 °C)	126	129	131	132	L
Avg $U_{per\ floor\ area}$	1.209				W/m^2.K
Household's internal capacitance	917.3				kJ/K
Floor area	87				m^2
Set temp. (22.00–07.00/ 07.00–22.00).	(16/20)				°C
Hot water tank volume	80				l
Emitters total water volume	42.03				
Emitters total surface area	20.54				m^2
Collector absorption coeff. (τα)	0.87				
Collector heat removal coeff. (F′)	0.89				
Collector total loss coeff. (K)	4.187				W/m^2.K
Absorber area per collector	2				m^2
Number of collectors	2				

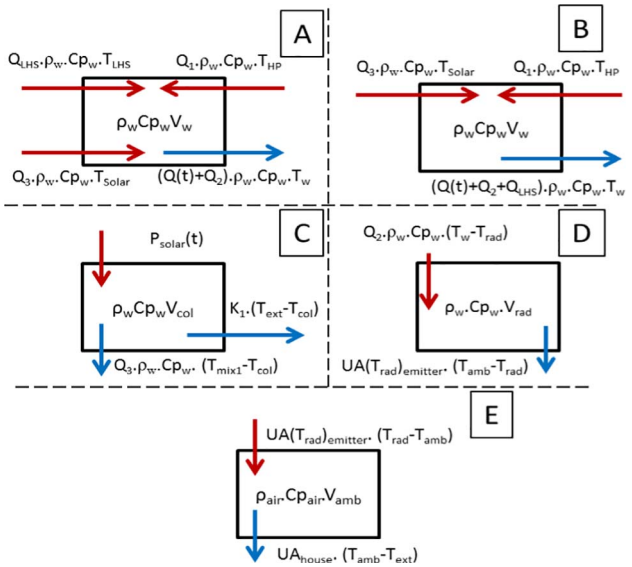


Fig. 8. Nodal balance equations for the hot water tank (A and B), the solar thermal collector (C), the emitters (D) and house (E) volumes.

It can be seen that the heat pump operates mainly during the winter months due to low solar radiation, being the required thermal energy provided almost entirely by the solar thermal collectors in the remaining months, due to the system's higher thermal storage capacity. The big temperature variations in the latent heat store mainly in the cold end side is consequence of its low water volume within the store (only 16 L) dropping steeply whenever a cold temperature inlet is presented either by the heat emitters of the grid water.

It can also be seen the PCM effect on the store's cold temperature rising steadily and converging near the PCM's melting point of 54 °C when there's no hot water consumption of no circulation through the heat emitters. Considerable thermal stratification was successfully achieved mainly due to the solar thermal input, proving to be beneficial when comparing with the conventional system from Mckenna's model [21].

The winter climate predictions demonstrated that the higher thermal capacity around 54 °C of the PCM allowed the latent heat store

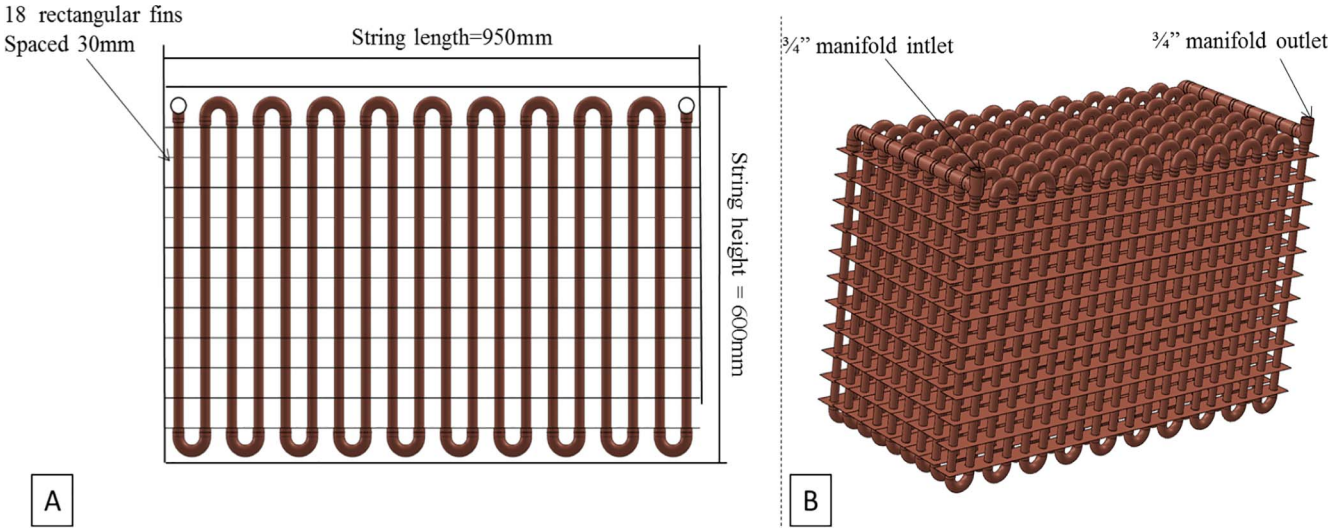


Fig. 9. Detailed section view of a single string (A) and isometric view of the store without rectangular enclosure (B).

Table 4
Latent heat storage system geometrical properties and heat transfer properties used in the numerical model.

Store width [mm]	450	HTF flow rates [l/min]	
Store length [mm]	950	Q0	20
Store height [mm]	600	Q1, Q2	12
Number of modules	10	Q3	4
Volume [L]	255		
PCM fraction (store/system) [%]	89/66	Tube diameter (OD/ID) [mm]	15.88/13.39
Spec HT area [m^2/m^3_{PCM}]	83.95	Reynolds (Re)	1176–5878
Number of fins	11	Prandtl (Pr)	3.50
Fins HT area increase [%]	274	Nusselt (Nu)	8–44
t insulation (EPS) [mm]	50	(h_{cv}) [W/m^2 K]	370–2106
λ insulation [W/m K]	0.034		
PCM (RT54HC)		PCM capacity (40–65 °C) [kWh]	11.61
Hs (40–51) [kWh/m^3]	6.79	Water + tube [kWh]	3.14
Hl (57–65) [kWh/m^3]	40.9	LHS/Water increase [%]	53
Hsl (51–57) [kWh/m^3]	4.10	Overcapacity (winter) [%]	20

to provide heat for two 8 h periods (from 05.00 to 13.00 and from 16.00 to 24.00) of space heating, successfully offsetting the heat pump operation to economy 10 low tariff periods, as seen in the red[1] curve of Fig. 12.

The seasonal solar fraction was calculated by combining the daily solar thermal collectors energy gains obtained in each simulation (when the solar pump P3 was activated).

Aggregating the results obtained for a yearly comparison, the solar fraction increased by 65% compared to the gas boiler system. Due also to the heat pump's coefficient of performance, the household's yearly energy consumption was 79% less than the conventional gas boiler system modelled by Mckenna.

The seasonal CO_2 emissions were calculated in the conventional system by multiplying the energy used in the gas boiler each day with the associated emissions of natural gas from [4], divided by the boiler efficiency (estimated to be 85% [24]). For the heat pump system, the electricity used by the heat pump in each second was multiplied by the correspondent grid emission value for the season calculated using Hawke's marginal emission factors [4], profiles seen in Fig. 1, and divided by the correspondent COP based on the ambient temperature [23].

The predicted reduction in carbon emissions based on the current grid emission values [1,4] for the heat pump systems with stores was 62% less. The obtained values could have been more promising using the salt hydrate eutectic mixture; however, corrosion and material segregation issues might limit the storage cycle reversibility [25].

4.1. Economical comparison of all modelled systems

In order to estimate a simple payback period for a 20 year life span, a market assessment was made to all the required components to install the proposed systems. In terms of heat source, Table 5 presents the capital difference cost of installing an air-source heat pump unit with solar thermal collectors to the conventional gas boiler unit. Based on the studies performed by Kelly et al. [26], installation costs were considered 5% of the initial capital expense (CAPEX) and operation and maintenance 1% of the initial CAPEX.

Table 5 also presents a general comparison for storage costs. For the hot water tank pricing, prices were retrieved from Mibec thermal solutions [33], and a linear interpolation defined the value for the specific volume in question. The compact latent heat storage presents a higher CAPEX, mainly due to requiring a considerable amount of copper tubing and solder fittings.

Table 6 presents the levelized cost of energy (LCOE) for each solution according to dwelling size. Eq. (14) presents the procedure used to determine, for a lifetime of 20 years [35] and an interest rate of 3.5%, the LCOE for each system (assuming a "zero-risk" investment), based on Smallbone et al. [35]. Gas and electricity (economy 10 [5]) prices were retrieved from SSE [36]. Economy 10 electricity tariff considered was 8.46p/kWh and gas tariff was 3.72p/kWh, both with a daily standing charge of 14.8 pence.

$$LCOE = \frac{\left(\frac{CAPEX \times r}{1-(1+r)^{-n}} + OPEX + Q_{used} \times E_{tariff}\right) \times n}{Heat_{produced} \times n} \times 1000\left[\frac{£}{MWh}\right]; \quad (14)$$

It can be seen that the LCOE for all storage systems reduces with increasing storage capacity; packed beds offer the lowest among the 3 storage solutions studied. Although the buffer tank presents the lowest CAPEX among the storage solutions studied, its LCOE is still higher than the other two storage solutions due to its lower energy savings. Gas boilers at current gas prices are still the most economical option, however they match the LCOE of packed bed if a carbon tax of 8.85£/ton is added to its fuel price, value still below the estimated by Brink et al. [37] of around 17£/ton for 2016.

Assuming the 11.54£/tonCO_2 applied to current natural gas boilers,

[1] For interpretation of color in Fig. 12, the reader is referred to the web version of this article.

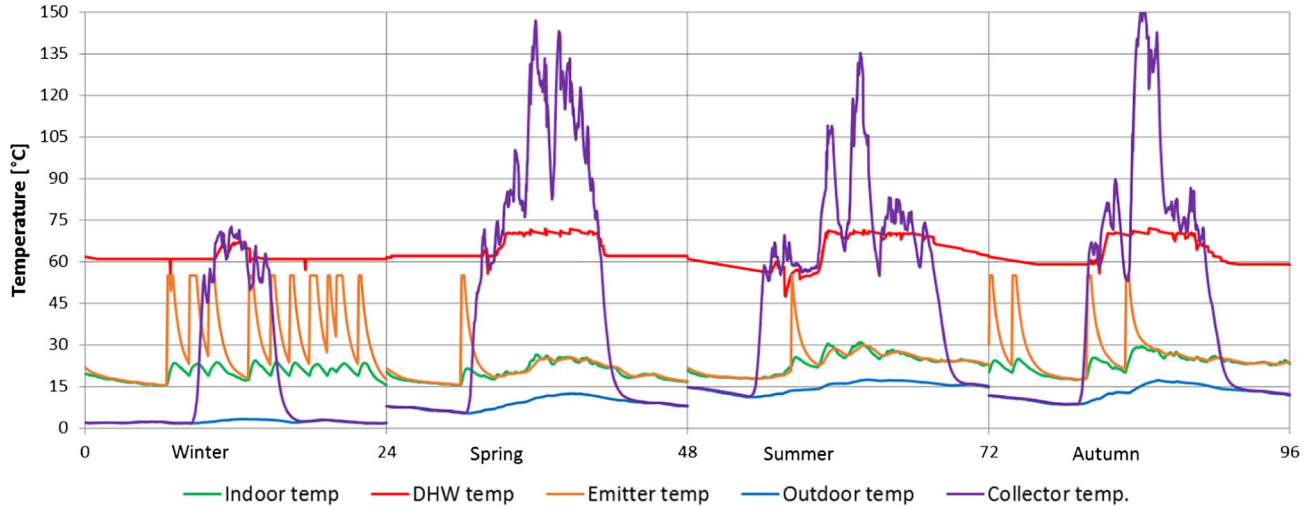


Fig. 10. Predicted daily temperatures and heat supply rates obtained using Mckenna's high resolution stochastic model [21] in all seasons.

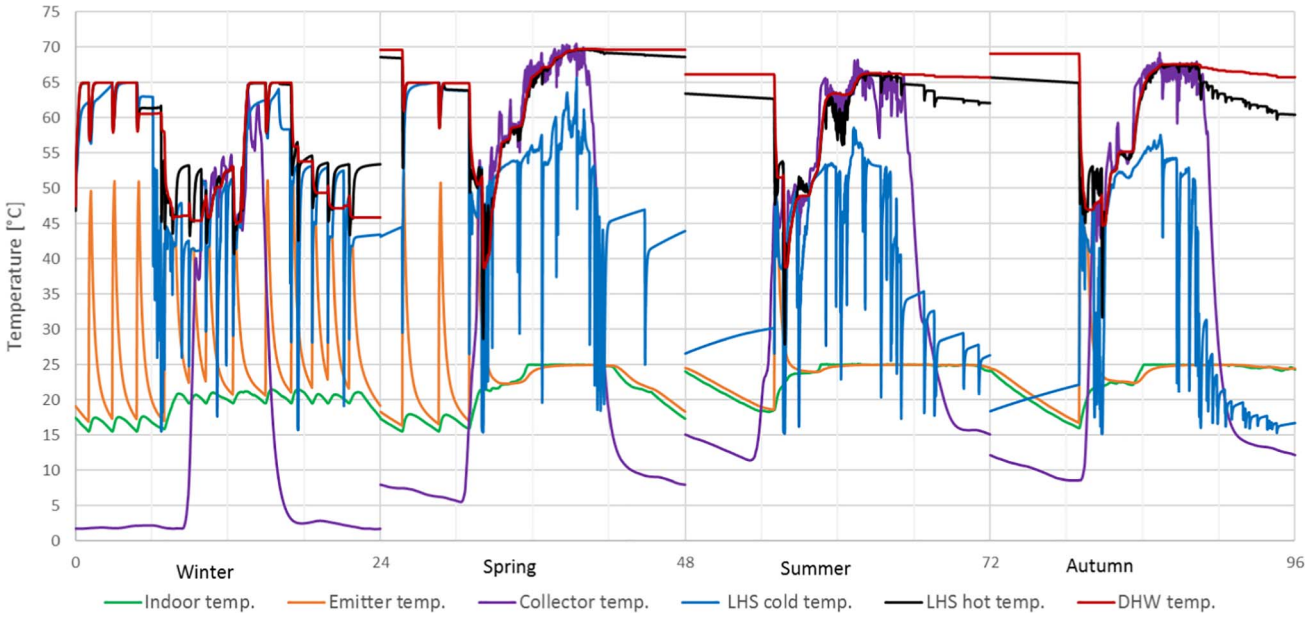


Fig. 11. Predicted temperatures and heat supply rates obtained with the PCM simulation.

value still below the assumed 17£/ton by the UK government [38], the payback was calculated for the replacement of current natural gas heating system using Eq. (15). To obtain a payback period of 8 years, the heat pump system would require a CAPEX reduction of 52%.

$$\frac{CAPEX \times r}{1-(1+r)^{-n_{payback}}} = \left(Savings_{year} - OPEX - \frac{CAPEX \times r}{1-(1+r)^{-n_{payback}}} - Q_{used} \times E_{tariff} \right) \quad (15)$$

5. Conclusions

Thermal stores including phase change materials have the potential to store larger amounts of thermal energy within a smaller temperature range compared to stores just using water. Due to the low thermal conductivity of many PCMs, poor rates of thermal diffusion within the PCM can reduce significantly the nominal storage system charge and discharge heat transfer rates.

Modifying the store geometry by allowing a parallel flow configuration among the latent heat storage modules reduces the flow passing through each module allowing a bigger thermal stratification.

The numerical model developed to evaluate the replacement of conventional gas fired boilers with heat pumps coupled with a PCM thermal store to offset heat pump operation from peak electrical demand periods in a semi-detached dwelling, predicted that yearly CO_2 emissions could be reduced by an average of 58% using current grid emission values. Accounting that these type of dwelling represents 25% of the British housing stock, a 58% reduction emission on these dwellings would represent a yearly reduction of 8.64 million tonnes of CO_2 if the system was integrated in the 6 million semi-detached dwellings in the UK, values that would increase if further efforts to decarbonize UK's electrical grid are taken.

Economically, the integration of PCM's into domestic hot water systems is a costly solution, using current energy prices, being the best levelized cost of energy obtained for heat pump with compact latent heat store 117.84£/MWh. A carbon tax to current natural gas consumption of 8.94£/ton CO_2 is required to equal the levelized cost of energy of natural gas to the latent heat storage system, for a 20 years life cycle value still below the assumed 17£/ton CO_2 by the UK government for 2016. If the initial capital expense is backed 33% by the

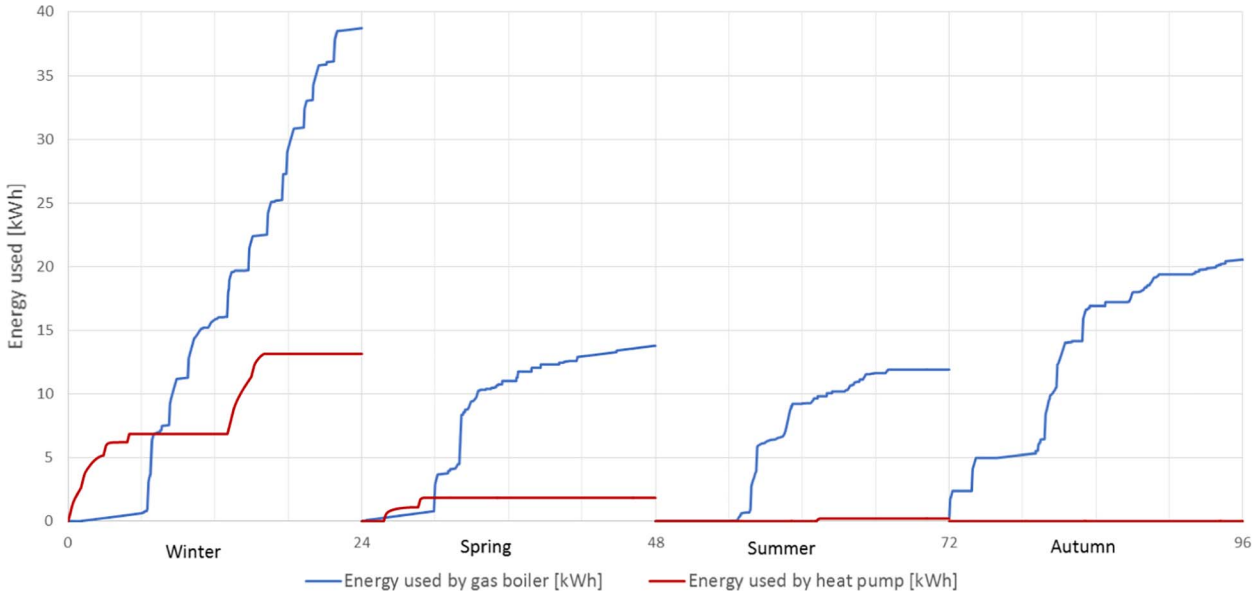


Fig. 12. Daily energy consumption comparison between the conventional gas boiler and the heat pump + latent heat store systems.

government, the heat pump system would payback itself in 8 years (assuming a carbon tax of 11.54£/tonCO_2 emitted for the gas boiler).

To meet the UK's 80% carbon emissions reduction targets by 2050, the electrification of current domestic water heating systems must be made. The increased peak electrical load generated by the electrification of heat can be moderated by using enhanced buffer tanks with their thermal capacity increased by including PCMs to allow operation of heat pumps to be time shifted to periods of low grid electrical load while still meeting heat demand and comfort requirements.

Table 5
Heating system price description of the heat pump and gas combi boiler systems.

Prices [£]	Component	Heat pump	Gas boiler	Reference
Solar thermal system	Thermasol (TS8001) panel	2 × 300		[27]
	Grundfos UPS pump	110		[28]
	Solar control box	164		[29]
	Hydraulics (tubing + valves + filters)	225		[30]
Air-source heat pump (Daikin Altherma)	11 kW Outdoor Unit (ERSQ011AV1)	2472		[31]
	11 kW Hydrobox (EKHBRD011ACV1)	2985		
Combi-boiler	Worcester combi boilers		1098	[24]
Labour costs	Installation costs	327.8	109.9	[32]
	Yearly maintenance	65.56	21.97	
Thermal store	120L hot water tank	225		[33]
	190 return bends	392		[30]
	120 m copper tube	229		
	4 h soldering	54		[34]
	255L of RT54HC	101		[7]
Heating system OPEX [£/year]		65.56	21.97	–
Heating system CAPEX		7838	2532	–

Table 6
Calculated levelized cost of energy, energy and CO_2 emission reductions per year for each system.

Yearly values	Heat pump system	Gas boiler system	Unit
Yearly heat used	6693		kWh/year
Yearly electricity used	1390	0	
Yearly gas used	0	5701	
Yearly CO_2 emitted	507	1163	kgCO_2/year
System COP	4.81	1.01	
Energy reduction	76	0	%
CO_2 reduction	56		
Tariff savings	163		£
LCOE (20-year cycle)	117.84	69.66	£/MWh

Acknowledgements

The research presented in this paper is funded by the EPSRC through Grant reference EP/K011847/1, the Interdisciplinary centre for Storage, Transformation and Upgrading of Thermal Energy (i-STUTE) and a Loughborough University funded PhD studentship.

Appendix A. Supplementary material

Supplementary data associated with this article can be found, in the online version, at http://dx.doi.org/10.1016/j.applthermaleng.2018.01.120.

References

[1] K. Harris, A. Annut, I. MacLeay, Digest of United Kingdom Energy Statistics 2017, vol. a. Crown, 2017.
[2] N.J. Hewitt, Heat pumps and energy storage – the challenges of implementation, Appl. Energy 89 (1) (2012) 37–44.
[3] National Grid. UK Future Energy Scenarios 2014. Energy, 2014, p. 220.
[4] A.D. Hawkes, Estimating marginal CO_2 emissions rates for national electricity systems, Energy Policy 38 (10) (2010) 5977–5987.
[5] N.J. Kelly, P.G. Tuohy, A.D. Hawkes, Performance assessment of tariff-based air source heat pump load shifting in a UK detached dwelling featuring phase change-enhanced buffering, Appl. Therm. Eng. 71 (2) (2014) 809–820.
[6] A. Beizaee, D. Allinson, K.J. Lomas, E. Foda, D.L. Loveday, Measuring the potential of zonal space heating controls to reduce energy use in UK homes: the case of unfurbished 1930s dwellings, Energy Build. 92 (2015) 29–44.
[7] Rubitherm Technologies GmbH, "Rubitherm GmbH," Rubitherm GmbH, 2016. [Online]. Available < http://www.rubitherm.eu/ > .
[8] G. Baran, A. Sari, Phase change and heat transfer characteristics of a eutectic mixture of palmitic and stearic acids as PCM in a latent heat storage system, Energy Convers. Manage. 44 (20) (2003) 3227–3246.
[9] Y. Sun, Magnesium Chloride Hexahydrate, Alibaba, 2017. [Online]. Available < https://www.alibaba.com/product-detail/Magnesium-Chloride-Hexahydrate-98-_495728300.html?spm=a2700.7724838.0.0.xCJ2OM&s=p > .
[10] Juan wang, Magnesium Nitrate hexahydrate Mg(NO3)2.6H2O (CAS 13446-18-9), Alibaba, 2017. [Online]. Available < https://www.alibaba.com/product-detail/98-Magnesium-Nitrate-hexahydrate-Mg-NO3_652554224.html?spm=a2700.7724838.0.0.PJjf1r&s=p > .
[11] Sting hong, Indonesia factory palmitic acid for feeding, Alibaba, 2017. [Online]. Available: < https://www.alibaba.com/product-detail/Indonesia-factory-palmitic-acid-for-feeding_1859997367.html?spm=a2700.7724838.0.0.vC9qbY&s=p > .

[12] I. Schuller, Plastic Rubber Cosmetic Grade/Stearic Acid, Alibaba, 2017. [Online]. Available < https://www.alibaba.com/product-detail/Plastic-Rubber-Cosmetic-Grade-Stearic-Acid_50032253807.html?spm=a2700.7724838.0.0.gqR1ME > .
[13] N. Ukrainczyk, S. Kurajica, J. Šipušiæ, Thermophysical Comparison of Five Commercial Paraffin Waxes as Latent Heat Storage Materials, vol. 24. 2010.
[14] C. Vélez, M. Khayet, J.M. Ortiz de Zárate, Temperature-dependent thermal properties of solid/liquid phase change even-numbered n-alkanes: n-Hexadecane, n-octadecane and n-eicosane, Appl. Energy 143 (2015) 383–394.
[15] F. Jep, Refined & Semi Refined Paraffin Wax 58/60, Alibaba, 2017. [Online]. Available: < https://www.alibaba.com/product-detail/Refined-Semi-Refined-Paraffin-Wax-58_50033585100.html?spm=a2700.7724838.0.0.pUWhgk > .
[16] TA Instruments, Discovery TA intruments Brochure. New Castle, DE 19720, United States, p. 10, 2015.
[17] M. Mazman, L.F. Cabeza, H. Mehling, M. Nogues, H. Evliya, H.O. Paksoy, Utilization of phase change materials in solar domestic hot water systems, Renew. Energy 34 (6) (2009) 1639–1643.
[18] K. Nakaso, H. Teshima, A. Yoshimura, S. Nogami, Y. Hamada, J. Fukai, Extension of heat transfer area using carbon fiber cloths in latent heat thermal energy storage tanks, Chem. Eng. Process. Process Intensif. 47 (5) (2008) 879–885.
[19] W. Wagner, VDI Heat Atlas vol. 2010, Springer, Berlin Heidelberg, 2010.
[20] K.J. Chua, S.K. Chou, W.M. Yang, Advances in heat pump systems: a review, Appl. Energy 87 (12) (2010) 3611–3624.
[21] M. Eoghan, T. Murray, CREST Demand Model, December 2015.
[22] DECC, English Housing Survey: HOUSEHOLDS 2015-16, 2016.
[23] Website of daikin Altherma High temperature heat pumps; 2015. [Online]. Available: < http://www.daikin.co.uk/domestic/needs/heating/air-water-heatpumps-ht/index.jsp > .
[24] D. heating supplies technical team, Worcester Combi Boilers. Direct Heating Supplies, March 2017.
[25] F.C. Porisini, Salt hydrates used for latent heat storage: corrosion of metals and reliability of thermal performance, Sol. Energy 41 (2) (1988) 193–197.
[26] J.A. Kelly, M. Fu, J.P. Clinch, Residential home heating: the potential for air source heat pump technologies as an alternative to solid and liquid fuels, Energy Policy 98 (Supplement C) (2016) 431–442.
[27] J.F. Kreider, F. Kreith, Solar Heating and Cooling: Engineering, Practical Design, and Economics, McGraw-Hill Book Company, New York, 1975.
[28] N. D. Jensen, H. Komossa, K.F. Nielsen, Circulating pump unit. Google Patents, March-1984.
[29] S. S. Uk, Solar thermal controller. WooCommerce, September-2017.
[30] T. Team, Screwfix, Screwfix Direct Ltd., September-2017.
[31] D. technical team, Daikin UK price list. Climate Center, March-2015.
[32] J.A. Kelly, M. Fu, J.P. Clinch, Residential home heating: the potential for air source heat pump technologies as an alternative to solid and liquid fuels, Energy Policy 98 (Supplement C) (2016) 431–442.
[33] M.T. Solutions, Buffer tanks. Web Expressions, September-2017.
[34] H. Capital, Soldering technician salary. Payscale, Inc., September-2017.
[35] A. Smallbone, V. Jülch, R. Wardle, A.P. Roskilly, Levelised Cost of Storage for Pumped Heat Energy Storage in comparison with other energy storage technologies, Energy Convers. Manag. 152 (Supplement C) (2017) 221–228.
[36] C. Amountzias, H. Dagdeviren, T. Patokos, Pricing decisions and market power in the UK electricity market: a VECM approach, Energy Policy 108 (Sep. 2017) 467–473.
[37] R. Martin, L.B. de Preux, U.J. Wagner, The impact of a carbon tax on manufacturing: Evidence from microdata, J. Public Econ. 117 (Supplement C) (2014) 1–14.
[38] DECC, The future of heating: a strategic framework for low carbon heat in the UK, Dep. Energy Clim. Chang. (2012).